Shrinkage behaviour of semi-crystalline polymers in Laser Sintering: PEKK and PA12

L. Benedetti*[a], B. Brulé[b], N. Decraemer[b], K. E. Evans[a], O. Ghita[a]

[a] *University of Exeter, College of Engineering, Mathematics and Physical Sciences, EX4 4QF Exeter, United Kingdom*
[b] *Arkema, Cerdato, Route du Rilsan, 27470 Serquigny, France*

Abstract

Shrinkage is extensively mentioned in the literature as one of the main causes for dimensional instability or poor performance in Laser Sintering (LS). This study proposes and examines a methodology to describe shrinkage in cooling from a material perspective. Thermal behaviour and crystallisation effects were measured to determine the influence of powder structure and density on overall LS shrinkage. PEKK and PA12 powders were used to assess such behaviour in LS. The shrinkage parameter associated with powder bulk properties has the greatest impact in PEKK, contributing to 57% of the total shrinkage observed in cooling for this material as supported by the low values of bulk density, irregular morphology and internal porosity observed for these particles. For PA12, crystallisation is responsible for 60% of the overall shrinkage observed. In LS, PEKK shows an overall shrinkage approximately 30% lower than PA12, which makes it a promising material for maintaining final part dimensions.

Keywords:
Laser sintering, Shrinkage, Powder bulk density, Crystallisation, PEKK, PA12.

1. Introduction

Laser Sintering (LS) is an Additive Manufacturing (AM) technique in which particles are bonded together by using a laser as heat source to create a 3D part, layer upon layer [1]. In comparison with conventional manufacturing, LS enables part customization and integration, quick manufacturing of complex and otherwise impossible geometries and the potential for generating serial products with reproducible properties without the need for costly tooling [2–5]. However, some limitations are found: porous surfaces, the need for finishing, size constraints, variation in machine and chamber temperatures and large shrinkage rates [3, 6, 7].

*Corresponding author.
Telephone number: +44 (0) 1392 725 831
E-mail address: lb636@exeter.ac.uk

1.1. Shrinkage behaviour in laser sintering and injection moulding

In conventional processes, e.g. Injection Moulding (IM), dimensional inaccuracy is mostly a result of high cooling rates [8, 9]. In Laser Sintering, other sources in addition to cooling may be causing dimensional mismatch such as the slicing process and machine resolution [10, 11]. Shrinkage during cooling, however, is the fundamental aspect preventing dimensional accuracy and part reproducibility, in some cases leading to curling and warping [7, 12–14]. For this reason, an optimal shrinkage factor is applied to compensate for the reduction in dimension.

In IM, the Shrinkage Factor for Polyamide 12 (PA12) varies from 0.7% to 2%. In the case of Poly(ether ether ketone) (PEEK), such values vary between 1.2% and 1.5%. Interestingly, shrinkage is significantly lower for IM Poly(ether ketone ketone) (PEKK), from 0.004 to 0.005%, due to its low degree of crystallinity [15, 16]. For LS, such values are highly dependent on the system and grade; for EOS PA2200 powder manufactured using a Formiga P100 system, the scaling factor accounts for a shrinkage in X, Y and Z of, respectively, 3.2%, 3.2% and 2.2%. For EOS PEK HP3, the recommended scaling factor in a EOS P 800 system is of 4.5% in all directions, but reduces to 3% in Z direction from 200 mm high [17]. For the case of PEKK, the scaling factors are not yet available, but in comparison with IM, the LS produces a complete crystalline sample as a result of the prolonged time of cooling.

As melting is constrained by the spot size of the laser in LS, consolidation hence shrinkage is significantly different from other conventional techniques. In IM, consolidation occurs from a polymer in liquid phase, whilst in LS the energy of the laser beam is focused to a punctual region on the bed. Furthermore, the solidification occurs in seconds for IM due to the possibility of high cooling rates being applied, which promotes a uniform structure. The cooling of LS parts is subdivided into a millisecond cooling once the laser scan is finished followed by a slow cooling which takes several hours, therefore promoting a different crystalline structure.

1.2. Laser sintering parameters influencing shrinkage

Few studies have attempted to explore the main causes of shrinkage in LS; Shi et al. [18] mentioned change in temperature, the process characteristics and crystallisation. Temperature shrinkage (β_T) is the shrinkage associated with the change in temperature when no phase transformation is observed. This value is an intrinsic property of the material and is assessed by means of linear expansion/contraction coefficient. According to Shi et al. [14], such shrinkage is insignificant when compared with the change in dimensions due to crystallisation.

Shrinkage due to process refers to the shrinkage associated with the parameters applied for manufacturing and the process selected. The parameters for LS include laser parameters - power, scan spacing, scanning speed, beam offset, scanned path, spot diameter - and machine parameters, such as layer thickness, temperatures, and in a minor scale, the recoating process. Negi and Sharma [10] studied the effect of laser power,

scan speed, scan spacing and scan length in shrinkage of LS PA 32000GF. By varying the scan speed from 2500 mm/s to 4500 mm/s, the extreme speed values tested, shrinkage increased by 4.75% (an increase of ∼70% in total shrinkage), whilst shrinkage increased only by 1.38% (equivalent to ∼20% increase in total shrinkage) when varying the power from 28W to 36W, the extreme values of power selected. When changing part bed temperature and scan spacing, these values are intermediate. They attributed the high effect of scanning speed in shrinkage to the temperature difference caused by the shorter time interval between the sintered and non-sintered region when having a high scanning speed; this leads to an expansion of the heat exchange area due to less exposure of the laser.

Kumar et al. [19] stressed the importance of maintaining a uniform bed temperature throughout manufacturing to avoid curling. In fact, temperature control throughout the bed is an issue reported by several studies. Nonetheless, shrinkage due to LS process can be significantly reduced when comparing parts of similar geometry manufactured with the same combination of laser parameters in the same trial and equipment [14].

Another particularity of AM hence LS is the layer-by-layer nature of the process; this leads to anisotropy especially in Z direction, which does not seem to be linear throughout manufacturing [11, 12]. Soe et al. [12] investigated the non-linearity of PA12 shrinkage in Z direction using a EOS P 700 equipment and concluded that optimal part placement, parameters control and management of material improve part accuracy but the elimination of non-uniform shrinkage in Z is still a challenge. A few studies mention the rough surface of LS parts as a result of adhesion of extra layers at the bottom and on the top of the LS object, which can lead to dimensional inaccuracy [20–22].

1.3. Crystallisation influence on shrinkage

Several studies mention crystallisation as the dominant factor causing shrinkage and leading to dimension inaccuracy [7, 14, 23–26]. This parameter is not present in amorphous polymers as they do not have a specific melting temperature (T_m) but show a progressive change in volume with temperature. Nevertheless, other limitations are found for processing amorphous materials as poor consolidation achieved in the final part and identifying the operation window for a successful processing [25, 27]. A schematic representation of change in volume for amorphous and semi-crystalline polymers is shown in Figure 1.

For semi-crystalline polymers, broader thermal processing window is preferable as it prevents rapid crystallisation and avoids distortion in LS. Hence, for commercially available materials, the main cause of shrinkage is crystallisation, which is the rearrangement of the chains into a structure with lower volume. A higher degree of crystallinity leads to higher shrinkage, whilst different crystalline structures lead to different change in volume and shrinkage. Van den Eynde et al. [23] found an overall shrinkage of 2.9% for LS polybutene-1 in the tetragonal structure, whilst the hexagonal structure of this polymorph, observed a few days after sintering, shrinks approximately 5.8%. For PA12 grades, EOS PA2200 and Arkema Orgasol,

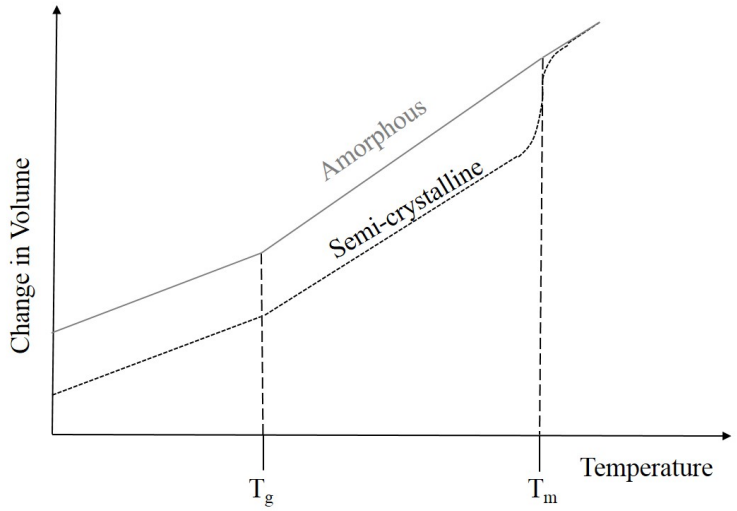

Figure 1: Comparison of change in volume between amorphous and semi-crystalline polymers.

Verbelen et al. [24] obtained a shrinkage of 4.7% and 4.6%, respectively.

Poly(aryl ether ketone)s (PAEKs) crystallize in the form of spherulites with an orthorhombic crystal structure. The degree of crystallinity can vary from 0% to 42% [28, 29]. Poly(ether ketone ketone) (PEKK) belongs to the PAEK family and also crystallises in the form of spherulites. Differently from PEEK, PEKK is a polymorph: in the primary structure (form I), phenyl-phenyl interactions among chains are aligned edge-to-face. In the secondary form (form II), the phenyl-phenyl interactions are aligned face-to-face [30]. According to Avakian et al. [31] and Blundell and Newton [32], form II is only obtained under solvent crystallisation or cold crystallisation. For Garcia-Leiner et al. [33], however, both forms can exist under certain conditions often encountered in LS and Fused Deposition Modelling (FDM) of PEKK.

Polyamide 12 (PA12) belongs to the polyamide family and has a degree of crystallinity ranging from 25% to 47% [34–36]. Most of the time this polymer presents a pseudo-hexagonal structure with a spacing of 0.42 nm, but being a polymorph, the monoclinic unit cell can be obtained and is associated with the α forms [37]. PA12 has four polymorphs named as α, α', γ and γ' [38]; the γ phase is the one obtained from the melt when cooled at atmospheric pressure. The γ' form is achieved upon fast quenching but transformed into γ when annealed, both γ phases present a hexagonal structure [37]. The α-form is obtained from high pressure, high temperature [39] or if the crystals from γ phase are heated above T_g but not increased further [35]. Van Hooreweder et al. [35] compared the crystallinity of LS PA12 with IM PA12 and found a slightly higher value on the degree of crystallinity for LS specimens, which they attributed to the slow cooling process. Interestingly, these specimens presented γ and α forms, whilst IM PA12 samples only showed γ phase due to the rapid cooling conditions.

In fact, the manufacturing technique selected displays a fundamental role in the morphology and degree

of crystallisation achieved in the final structure. For LS, crystallisation can be significantly different due to its prolonged cooling-annealing stage. This avoids distortion caused by abrupt changes in temperature but promotes a highly ordered crystal structures, hence shrinkage [7, 27].

1.4. Powder influence on shrinkage

Although crystallisation is of great concern in shrinkage, other intrinsic properties of polymers are crucial to guarantee dimension accuracy and final performance. Too low viscosity, for instance, can result in high levels of shrinkage due to the low molecular weight. Smaller polymer chains are easily arranged hence leading to higher shrinkage [7, 27]. The bulk density of the powder bed can affect consolidation. A more compact powder at room temperature is likely to have less voids at the processing temperature, which facilitates a fully solid 3D structure in which less shrinkage is observed. Finally, spherical particles [25, 40] with a narrow particle distribution and an average size of 60μm [41, 42] are preferred to promote a uniform consolidation, minimize porosity and guarantee dimensional accuracy.

In literature, shrinkage was investigated when associated with processing parameters or location/ orientation in the LS system; only a general idea is found for shrinkage originated from different material properties. This study is the first study to experimentally measure the main causes of shrinkage during cooling for PA12 and PEKK in LS. Knowing the impact of each of the variables in the overall shrinkage helps understand the behaviour of PA12 and PEKK in the LS process, but also enables optimizing mechanical properties and dimensional accuracy.

This study does not attempt to evaluate the change in shrinkage for parts with different geometries or more complex design - all the experiments were performed with very simple geometries to account for material shrinkage during LS cooling only. In a similar way, one combination of laser parameters and temperatures was selected for each material to avoid other variables in the system. The authors are aware that the temperature distribution within powder bed systems is not always consistent. To account for any temperature fluctuations within the bed, the parts were placed at various locations.

2. Shrinkage equation

When a fully solid semicrystalline thermoplastic polymer is exposed to heating, expansion will occur. If the same material is subjected to cooling, shrinkage is observed. Most of the time, however, semicrystalline polymers do not come back to their original dimension as they are affected by the kinetics of crystallisation. In LS, the degree of crystallinity after cooling can be higher than before the melt due to the prolonged time given for the molecules to arrange in an organized structure. Therefore, this study will concentrate on the cooling between molten polymer and solid polymer/part as shown in Figure 2.

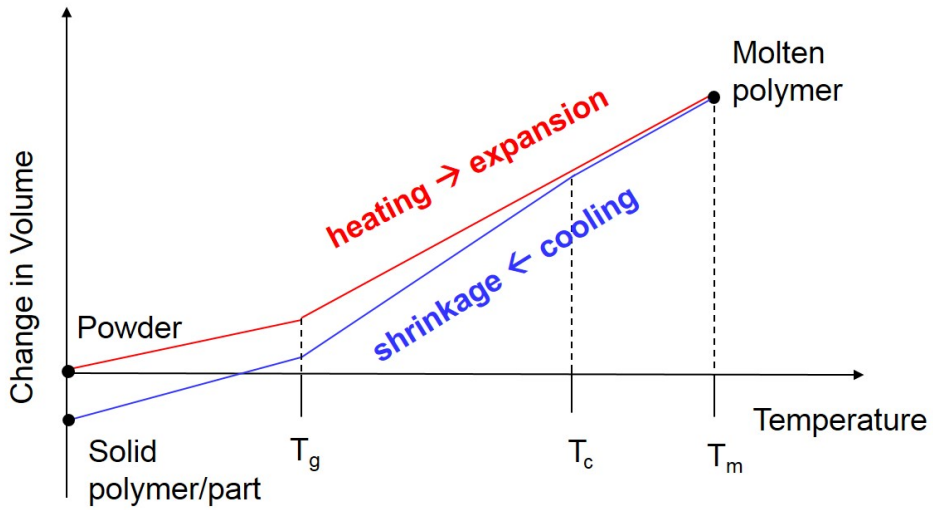

Figure 2: Change in volume with heating and cooling.

In addition to the kinetics of cooling, the particles in the LS bed are not fully compact and present a degree of porosity at room temperature and at bed temperature. This leads to a lower expansion while heating and may affect cooling. To take all these factors into account, equation 1 was proposed:

$$\beta_{total} = \beta_T + \beta_c + \beta_{powder} \tag{1}$$

In which β_T is the shrinkage caused by the change in temperature, β_c corresponds to the shrinkage due to crystallisation and $\beta powder$ is the shrinkage resultant from the powder bulk and particle characteristics at bed temperature, as it concerns only about shrinkage during cooling.

This equation aims to measure the effect of powder bulk in overall shrinkage during cooling. β_T is an intrinsic property of the material and it concerns the shrinkage when subjected to changes in temperature. This parameter was assessed using a DMA equipment operating in compression mode. β_c was measured using a TMA equipment in dilatometry mode and evaluating the changes in dimension within the material crystallisation range. Finally, β_{total} was calculated by producing specimens in LS systems and measuring their dimension.

3. Materials and methods

3.1. Materials

Two polymer families in Laser Sintering were selected for this study: PAEKs and Polyamides. The PAEK is a commercially available LS grade provided by Arkema as Kepstan 6000 PEKK grade [43]. This is a poly(ether ketone ketone) (PEKK) material prepared at a concentration of 60/40 T/I of terephthalic acid

(T) with para phenyl links and isophthalic acid (I) with meta phenyl links [44]. The PA12 grade used is the commercially available Orgasol PA12 also provided by Arkema. A general value for the glass transition temperature (T_g) and melting temperature (T_m) of these materials are listed in Table 1 [36, 43].

Table 1: Properties of PA12 and PEKK.

Grade	T_g [°C]	T_m [°C]
PEKK[43]	160	300
PA12[36]	55	177

3.2. Scanning Electron Microscopy (SEM)

A Hitachi S-3200N scanning electron microscope was used at an accelerating voltage of 10kV and current of 0.13nA. The samples were coated with 10nm layer of gold and images at magnitudes of 1000 and 2500 times were captured.

3.3. Particle Size Distribution (PSD)

PSD test was performed using a Malvern Mastersizer 3000E laser diffraction equipment. For PEKK polymer, a small sample of powder was dispersed at room temperature in a liquid solution of 0.4% of sodium hexametaphosphate to prevent the stabilization of bubbles while measuring particle size. For PA12, only water was used as solution. The test was repeated three times for each sample, with five measurements collected at each repeat.

3.4. Conditioned Bulk Density

Conditioned Bulk Density (CBD) values were measured using a Freeman FT4 powder rheology equipment whilst running flow properties test. This test used a 25ml split vessel and a metal blade rotating at both directions to create a pre-conditioned state by removing the excess of air trapped in the bulk. To measure CBD, the vessel is splitted to constrain the volume. Three measurements were performed for each material.

3.5. X ray diffraction

X-ray diffraction analysis (XRD) was performed on PEKK LS parts and PEKK powder for comparison reasons and morphology investigation. The analysis used a Bruker D8 Advanced X-Ray Diffractometer with Cu Kα (γ = 0.1542 nm) radiation and a LynxEye detector operating at a voltage of 40 kV and a current of 40 mA. The data was collected in a fixed time mode (1 s) with a step size of 0.05° and run from 2θ = 4 to 65°. Five measurements were performed for each - PEKK powder and LS PEKK parts. The data was processed using Jade 6 software.

3.6. Measuring β_{total}

Two different systems were used to produce LS specimens. Kepstan 6000 PEKK was processed in an EOSINT P800 High Temperature LS system [45], whereas Orgasol PA12 specimens were manufactured using an EOS Formiga P100 system [46]. The parameters selected for each are found in Table 2. As this study attempts to assess shrinkage due to material behaviour, all parts were manufactured with no scaling factors applied. However, beam offset was considered (Table 2), as it is a parameter dependent on laser spot size only.

Table 2: Laser sintering parameters for PEKK and PA12.

Parameters	Material	
	Kepstan 6000 PEKK	Orgasol PA12
Fill laser power (contour)	8.5 W	16 W
Scan speed (contour)	1000 mms^{-1}	1500 mms^{-1}
Beam offset	0.39 mm	0.19 mm
Energy density (hatching)	23.5 $mJmm^{-2}$	42 $mJmm^{-2}$
Layer thickness	120 μm	100 μm
Part bed temperature	292 °C	168 °C

The authors considered the anisotropic effect of LS process extensively reported in literature [11, 12, 47, 48] by producing parallelepipeds of different heights to account for the dimension differences found in Z axis. The dimensions chosen for X and Y are of 10 mm each, whilst Z axis varied from 10 mm to 100 mm in a 10 mm interval. Two parallelepipeds were produced for each height, one locally centralized in the manufacturing build, the other closer to the corners to account for potential temperature differences. A total of 20 parallelepipeds were manufactured for Kepstan 6000 PEKK and Orgasol PA12.

All samples were produced using the standard parameters available in Table 2 and the cooling process set by the manufacturer for each equipment. The cooling rate of LS PA12 is approximately 0.5 °C/min, as stated by Verbelen et al. [24]. Ghita et al. [49] mention a cooling rate of 0.2 °C/min for PEK HP3 manufactured in EOSINT P 800. For Kepstan 6002, the cooling rate was estimated based on the software measurements to vary between 0.1 and 0.5 °C/min. The parallelepipeds were then removed from the build and had their dimensions measured with the assistance of a calliper and a micrometer. Three measurements were performed for each parallelepiped and compared with the .STL file.

3.7. Measuring β_T

A Mettler Toledo DMA STARe System was used in the Compression Sample Holder configuration to enable Thermo Mechanical Analysis. This test aims to measure the shrinkage of the material during cooling due to change in temperature and not phase transformation. For this reason, no melting is achieved. Two cubic samples 2 x 2 x 2 mm^3 were tested for each material.

The cubes of Kepstan 6000 PEKK were produced using Injection Moulding in order to obtain a fully amorphous structure, therefore enabling the separation between shrinkage due to temperature from shrinkage due to crystallisation. The cubes were heated at 1.5°C/min from 25°C to 292°C and remained at 292°C for 10 min. This corresponds to the bed temperature used to manufacture PEKK in the EOSINT P800 High Temperature LS system used in this study. The cooling stage was carried out from 292°C to 25°C. To maintain the amorphous structure during cooling, liquid nitrogen was dispersed around the chamber. The cooling with nitrogen reached a rate of approximately -5°C/min and the full cooling profile was used to measure the coefficient of thermal contraction.

For Orgasol PA12, the cubes were manufactured by LS under the same conditions and parameters used to produce the parallelepipeds described in Section 3.6. The cubes were heated at 1.5°C/min from 25°C to 168°C and remained at 168°C for 10 min. This temperature was chosen as it is the recommended bed temperature of this grade when processed by a EOS Formiga P100 LS system. The cooling stage was performed at the same rate, 1.5°C/min (30% of the cooling rate used for PEKK), from 168°C to 25°C as fully amorphous structure is not achieved with Orgasol PA12. The full cooling profile was selected to measure the coefficient of thermal contraction.

3.8. Measuring β_c

This test was performed to assess full shrinkage at cooling from the melt, focusing on shrinkage due to crystallisation. A TA Instruments Q400 TMA was used in the compression mode with a flat-tipped dilatometer probe of 3 mm in diameter. Two different methods were chosen, a rapid cooling method and a slow cooling method. In the case of the slow cooling method, the cooling rate chosen to monitor crystallisation, although not exactly the same cooling rate as LS, which is not linear and difficult to monitor especially at high temperatures, has comparable rates and so far provides the best method to assess shrinkage occurring in LS. They are described in Table 3.

During the cooling stage of the rapid cooling method, liquid nitrogen was dispersed around the furnace, resulting in an approximate cooling rate of 55°C/min. The maximum temperature for rapid cooling method is higher than for slow cooling method to compensate for any possible thermal lags. The samples of Kepstan 6000 PEKK were produced using a cubic iron mould of 5 x 5 x 5 cm^3. The mould was half filled with powder and compressed with the assistance of a Universal Shimadzu AGS-X Series Tensile Tester. The force selected

Table 3: Methods for dilatometry analysis.

Grade	Slow cooling	Rapid cooling
Kepstan 6000 PEKK	• 25 °C to 292 °C at 20 °C/min • 292 °C to 303 °C at 0.5 °C/min • Remain at 303 °C for 5 min • 303 °C to 25 °C at 0.5 °C/min	• 25 °C to 380 °C at 20 °C/min • 380 °C to 25 °C at quick liquid nitrogen cooling

was close to 20kN and the powder remained under compression for 12 h. After removal, the samples were cut from the block into cubes of 5 x 5 x 5 mm^3. Three repeats were performed for each method.

To check the density, the samples were weighted and accurately measured using a micro-CT X-Tek Bench top CT 160 Xi (X-Tek Systems Ltd/Nikon Metrology UK Ltd, England) with a current of 65 μA, voltage of 65kV, pixel size of 3 μm and 360 ° rotation. Once the test was finished, the cooling profile was extracted and the region of crystallisation was selected to measure shrinkage. The changes in dimension found between 292°C and 200°C was attributed to crystallisation of PEKK. On visual inspection, the PEKK samples were opaque, a typical sign of crystalline morphology.

4. Results and Discussion

4.1. SEM

Kepstan 6000 PEKK and Orgasol PA12 pictures were captured at 500x and 2500x of magnification as shown in Figure 3.

For Kepstan 6000 PEKK, heterogeneous particles with porous structure and rough morphology is observed. The morphology of Orgasol PA12 approaches a spherical shape with almost no porosity and homogeneous structure throughout the particles.

4.2. PSD

The particle size and distribution curve and cumulative data are presented, respectively, in Figure 4 and Table 4.

PEKK shows a broad particle distribution with an average particle size slightly bigger than 50 μm, whilst Orgasol PA12 shows a narrower distribution with an average particle size of 40 μm. Both grades, however, are in the ideal size and distribution desired for LS particles [41, 42].

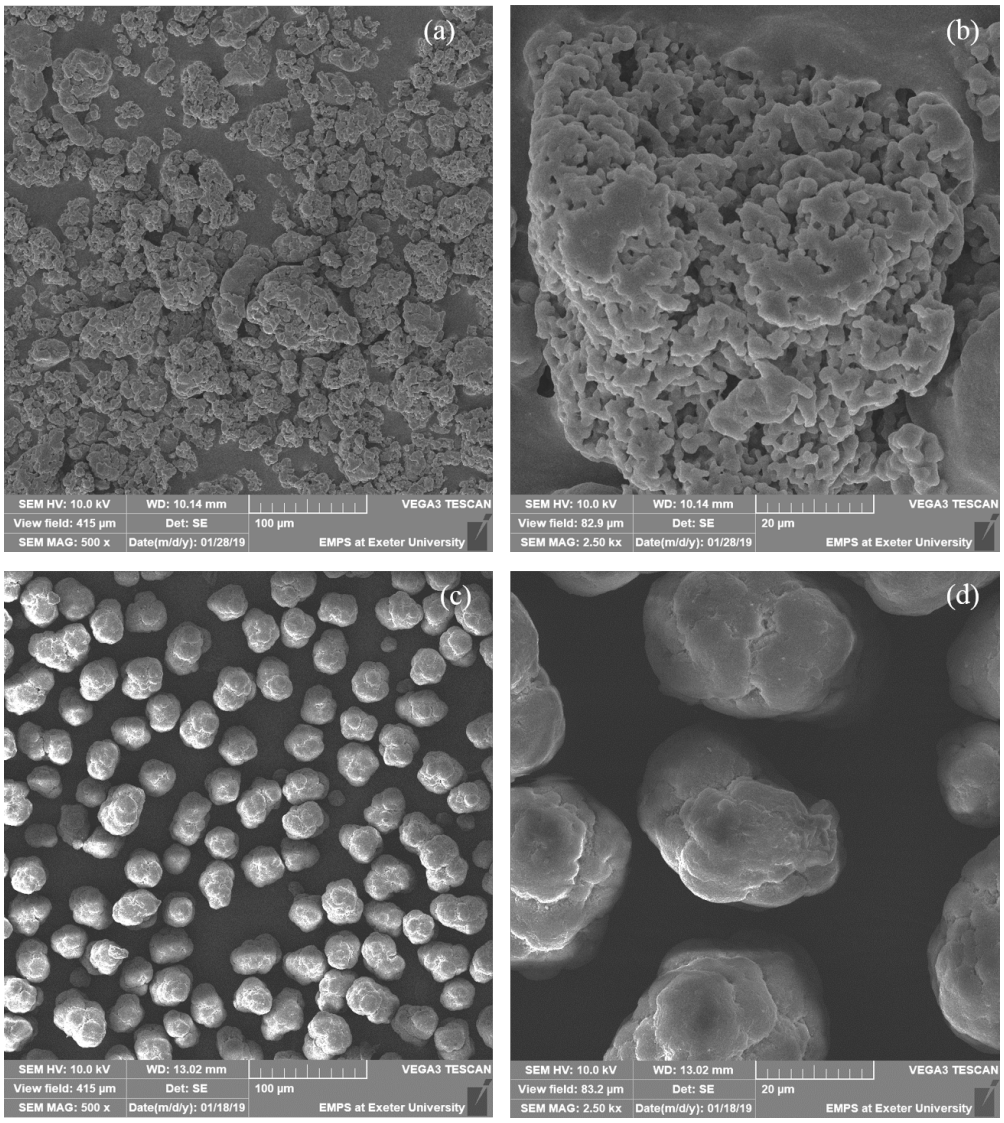

Figure 3: SEM images for PEKK (a) at 500x and (b) at 2500x and Orgasol PA12 (c) at 500x and (d) at 2500x.

4.3. Bulk density

CBD values were computed at room temperature and the results are found in Figure 5.

The values of CBD for PEKK are of 0.37 g/cm^3, which shows poor compact structure unless pressure is applied. The values of CBD for Orgasol PA12 are of 0.54 g/cm^3, slightly above the range for LS materials currently available [50], suggesting a good powder compact and even better performance. CBD is highly associated with particle morphology and porosity in the bulk and inside the particles. Figure 3 shows PEKK particles with rough morphology and high porosity, which supports the lower values of CBD shown in Figure 5.

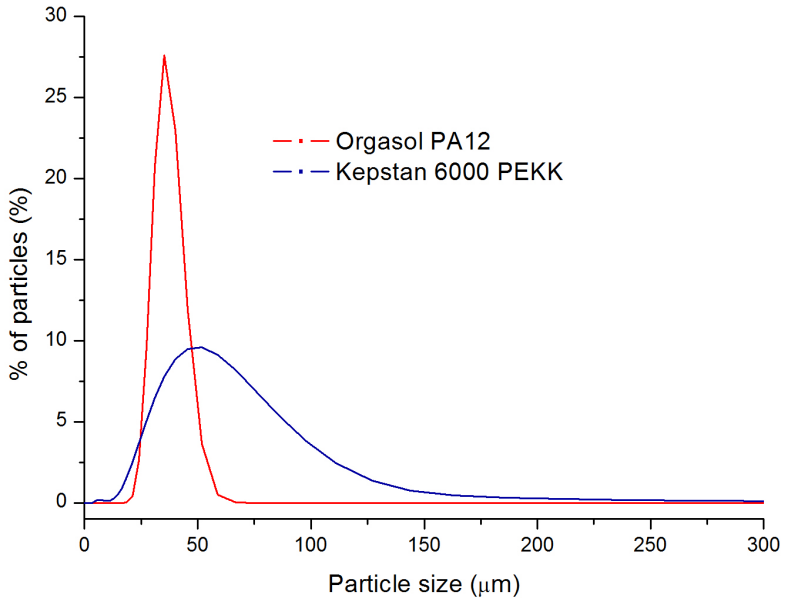

Figure 4: Particle size and distribution curve for PEKK and PA12.

Table 4: Particle size and distribution data for PEKK and PA12.

Material	Dx (10)	Dx (50)	Dx (80)	Dx (90)
Kepstan 6000 PEKK	26	52.8	83.5	181.6
Orgasol PA12	30.1	38.2	44.7	48.6

4.4. Parameters results

4.4.1. Shrinkage in laser sintering: β_{total}

The parallelepipeds were measured individually and the average shrinkage in Z axis for each height are shown in Figure 6.

Most of Orgasol PA12 parallelepipeds show a shrinkage around 2% in Z direction. Such shrinkage is visible from 10 mm but seems to achieve a plateau at 40 mm. Several factors may be contributing to this, such as crystallisation, thermal contraction and powder characteristics. Parallelepipeds with lower heights, however, show a significantly lower shrinkage; this might be due to the layer-by-layer nature of LS process but especially the downskin and upskin effect, which corresponds to the adhesion of extra layers at the bottom and on the top of the sintered object, respectively, due to the transmission of laser energy beyond the sintered layer of particles (downskin effect) and the adhesion of extra layers resultant from melting of

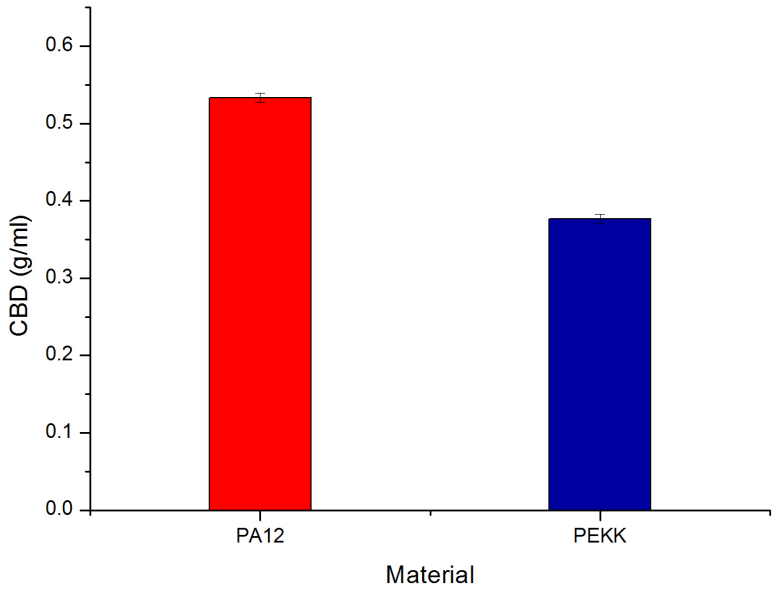

Figure 5: CBD values for PA12 and PEKK.

the upper layer (upskin effect) [20–22]. From 40 mm, the upskin and downskin effect assumes a linear and controllable behaviour and can be negligible.

Kepstan 6000 PEKK presents a more pronounced upskin and downskin effect and parallelepipeds of 10 mm height showed an expansion in Z axis during cooling. This effect is present for greater heights too, but seems to achieve a plateau around 3% of shrinkage from parallelepipeds of 50 mm height. The authors believe that, from this height, upskin and downskin effect is negligible and the acting factors on overall shrinkage are thermal contraction, powder characteristics and crystallisation just as for Orgasol PA12. Interestingly, once the plateau is achieved, the shrinkage observed in Z axis for PEKK is greater than for PA12.

Shrinkage was monitored in X and Y direction as well, and a final volumetric shrinkage was computed. This volumetric shrinkage considered the values for all the parallelepipeds in X and Y and the Z heights after achieving a plateau, which is at 40 mm for PA12 and 50 mm for PEKK. The results are shown in Table 5.

The shrinkage seems to be slightly higher at Y direction than at X direction for PEKK and PA12 parallelepipeds, but greater difference is visible for PEKK. This can be associated with powder spread and arrangement in the bed and the sintering strategy in EOS P800 LS systems. The final volumetric shrinkage is higher for PA12; this can be attributed to the intrinsic properties of this material as crystallisation and thermal contraction, which is known to be higher than for PEKK [36]. In Z direction, however, PEKK seems to have a greater shrinkage and is possibly associated with the layer-by-layer nature of LS process

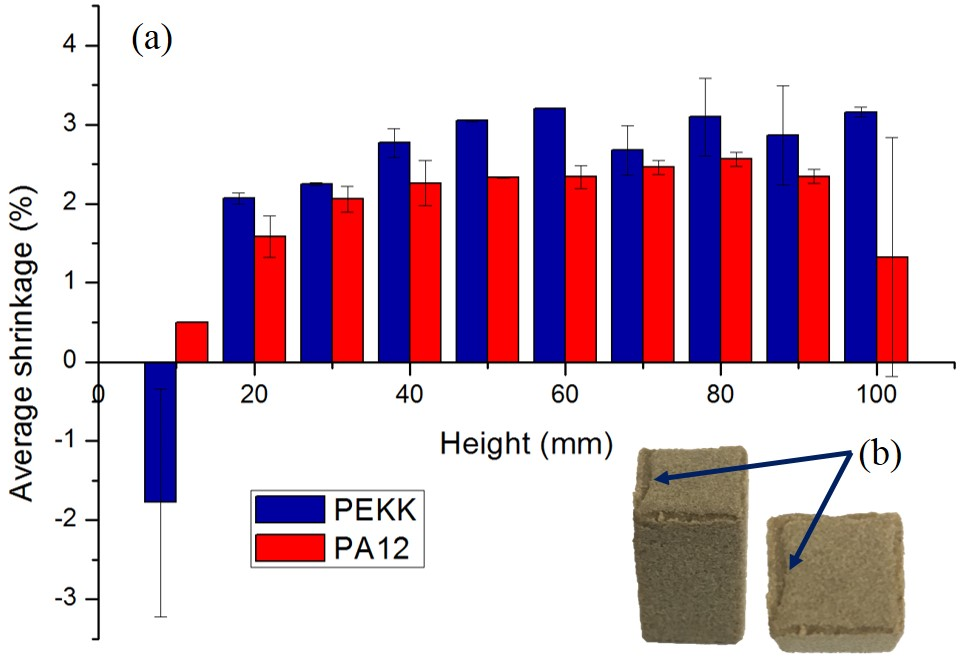

Figure 6: (a) Shrinkage of PEKK and PA12 parallelepipeds in Z direction; (b) downskin and upskin effect of PEKK.

and powder structure.

4.4.2. Shrinkage due to thermal contraction: β_T

One of the parameters considered in equation 1 is shrinkage due to thermal contraction (β_T); it consists on the shrinkage caused by temperature change during cooling not accounting for phase transformation. This parameter was calculated as described in Section 3.7 and the coefficient of thermal contraction and the overall shrinkage are presented in Table 6.

The results are close in value to literature for thermal expansion coefficient [36, 43]. The shrinkage of amorphous PEKK has a significantly lower value than the PA12. Kepstan 6000 PEKK overall shrinkage corresponds to approximately 10% of the shrinkage visible in LS, whilst this value is of 18% for PA12.

4.4.3. Shrinkage due to crystallisation: β_c

Shrinkage due to crystallisation is the parameter measuring the degree of chain arrangement and crystal morphology in the overall effect of material shrinkage. Figure 7 shows the crystallisation obtained for slow (a) and rapid (b) cooling methods described in Table 3 for Kepstan 6000 PEKK. The slow cooling method provided a significant decrease in dimension at the crystallisation range of this polymer, with an average of 1.77% shrinkage with the three repeats performed. The repeat measurements vary due to several factors: sample preparation, level of porosity within the sample at the end of the experiment and slight variation in cooling rate. The change in dimension is negligible for the rapid cooling method - Kepstan 6000 PEKK is

Table 5: Average shrinkage in laser sintering of PEKK and PA12

Material	Shrinkage in laser sintering (%)				
	X (10 - 100 mm)	Y (10 - 100 mm)	Z (10 - 100 mm)	Z (50/40 - 100 mm)	Volumetric
PEKK	1.14 ± 0.12	1.39 ± 0.14	2.34 ± 0.13	3.01 ± 0.15	5.45 ± 0.07
PA12	2.72 ± 0.007	2.85 ± 0.006	1.98 ± 0.3	2.23 ± 0.36	7.6 ± 0.17

Table 6: Thermal contraction during cooling.

Parameters	Materials	
	Kepstan 6000 PEKK	Orgasol PA12
Coefficient of thermal contraction [$^oC^{-1}$]	6.48 $\times 10^{-5}$	1.2 $\times 10^{-4}$
Overall thermal shrinkage [%]	0.55 ± 0.02	1.41 ± 0.35

usually amorphous when cooled at rates above 5°C/min. This is supported by the amorphous behaviour of this material when processed by conventional techniques, e.g. extrusion calendaring, thermoforming or IM. Polyamide, on the other hand, crystallises quickly even at high cooling rates and when processed by other manufacturing techniques.

Table 7 shows the average value measured for Kepstan 6000 PEKK using slow cooling method and the data achieved by Verbelen et al. [24] for Orgasol PA12. In the case of Verbelen et al., the experiment was slightly adapted to compensate the high flowability of PA12 [51]. PEKK, on the other hand, is a highly self-supported polymer which flows significantly less when subjected to melt.

Table 7: Crystallisation shrinkage of Kepstan 6000 PEKK and Orgasol PA12 [24].

Parameter	Materials	
	Kepstan 6000 PEKK	Orgasol PA12
Overall shrinkage due to crystallisation [%]	1.77 ± 0.5	4.6[24]

The measures match the expected crystalline behaviour of PEKK and PA12. The degree of crystallinity of PA12 is usually higher than PEKK, suggesting a higher degree of shrinkage at cooling from melting. Furthermore, PA12 γ phase presents a hexagonal structure whereof packing factor is higher than the orthorhombic crystal structure observed in PEKKs. For PEKK powder and PEKK LS parts, the XRD data

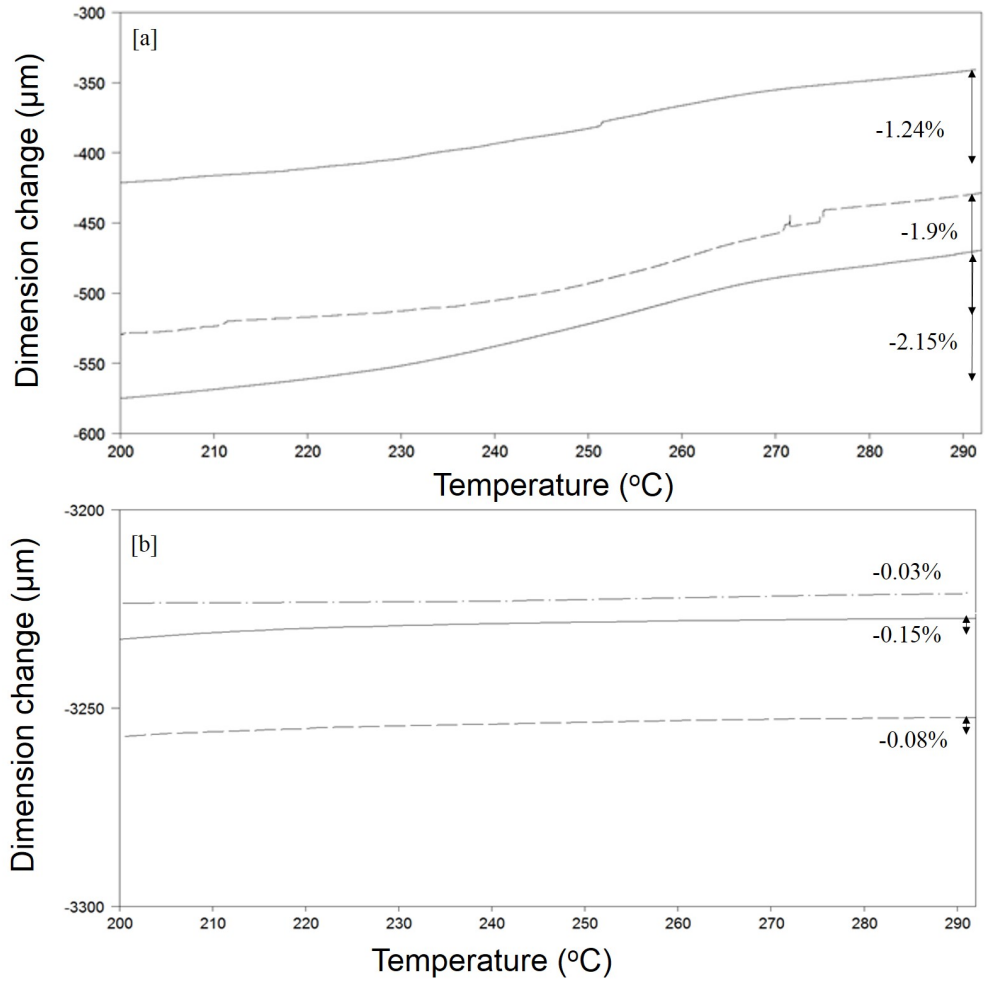

Figure 7: Dimension change due to crystallisation of Kepstan 6000 PEKK; [a] Slow cooling method; [b] Rapid cooling method.

(Figure 8) shows the presence of Form I. However, the vague peak at [010] seems to indicate the presence of Form II in the powder [30].

Describing cooling in LS remains a challenge as it is not uniform and occurs at different stages: during manufacturing, after manufacturing until it reaches T_g and below T_g. This methodology, however, considers this issue by choosing similar cooling rates achieved during the crystallisation of PEKK. Such cooling is high enough to prevent PEKK flowability affecting the data on crystallisation but is still within the limit of the TMA equipment.

4.4.4. Calculation of the powder bulk: β_{powder}

The experimental data measured for all of the parameters found in equation 1 were presented except for shrinkage due to powder bulk. This parameter describes the effect of powder compaction in shrinkage during cooling and is a combination of particle size, distribution, morphology, degree of porosity and arrangement

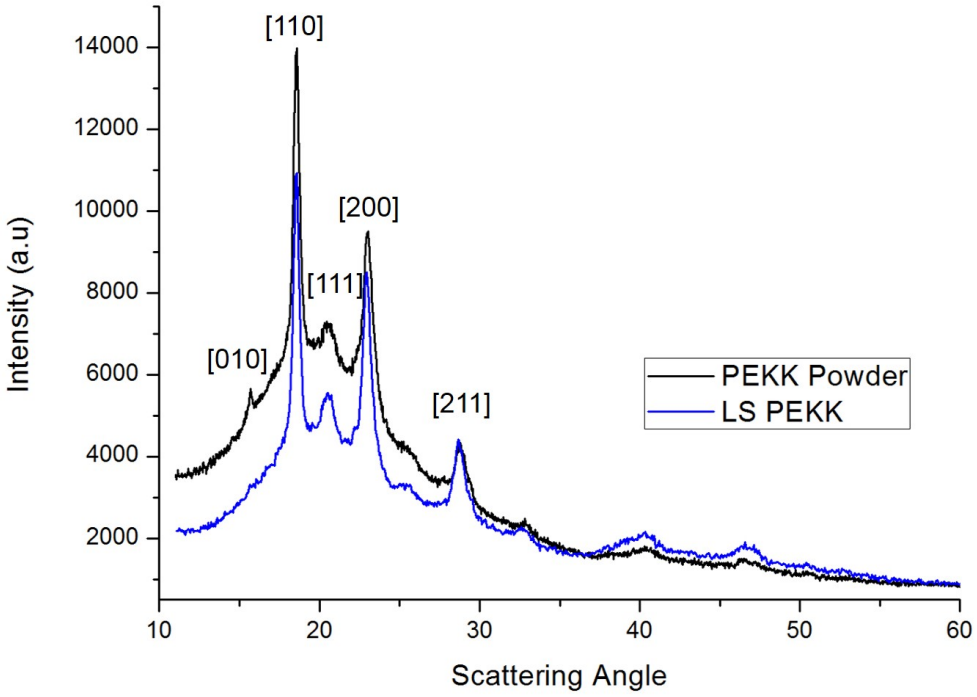

Figure 8: X-ray diffraction of PEKK powder and LS PEKK.

on the bed. In fact, particles have a very complex effect in LS and several studies attempted to assess this effect [25, 52, 53]; most of them considered particles at room temperature having the same behaviour as particles at bed temperature, which corresponds to the processing temperature. In this study, equation 1 aims to measure the effect of powder characteristics in final shrinkage at cooling from a material perspective, starting from bed temperature used in LS. This value was calculated for Kepstan 6000 PEKK and Orgasol PA12; the summary of shrinkage values are presented in Table 8.

Table 8: Shrinkage (%) in Laser Sintering and the effect of powder bulk.

Material	$\beta_{total}=$	β_c	β_T	β_{powder}
Kepstan 6000 PEKK	5.45	1.77	0.55	3.13
Orgasol PA12	7.6	4.6	1.41	1.59

The effect of shrinkage due to powder bulk is almost twice larger for Kepstan 6000 PEKK than for Orgasol PA12; this shrinkage is equivalent to almost 58% of the overall LS shrinkage during cooling of PEKK, whilst it corresponds to 21% of the overall shrinkage found for Orgasol PA12. These values are supported by the poorer CBD values of PEKK shown in Figure 5 and the rough and porous powder structure of this material when compared with PA12 powder (Figure 3).

Powder characteristics are extensively linked with powder flow and final part consolidation [54], but few studies mention shrinkage and potential changes in final part dimension [55] as a result of powder structure. The values presented show that powder characteristics also affect overall shrinkage and it can be controlled to a certain extent by having rounder particles, lower porosity and appropriate particle size and distribution.

5. Conclusions

This study aimed to identify and measure the effect of different polymer properties in overall material shrinkage during cooling in LS. A methodology was proposed by the authors and the shrinkage parameters were experimentally measured for Kepstan 6000 PEKK and Orgasol PA12, both grades provided by Arkema. With the measured parameters, shrinkage due to bulk density was assessed for each grade.

Depending on the material and powder characteristics, the shrinkage factors are different. Whilst crystallisation has the greatest impact in PA12 overall shrinkage during cooling, this parameters contributes to 32% of the overall shrinkage for PEKK. Previous literature highlights crystallisation as a factor preventing good dimensional accuracy in final polymeric parts; hence, a lower degree of crystallinity would lead to less warpage and a better dimension control.

Most of the shrinkage found in PEKK (58%) was attributed to powder bulk, a parameter associated with powder structure - porosity, morphology, size and distribution. For Orgasol PA12, such parameter contributed to 21% of overall shrinkage. These values are supported with SEM images, PSD and CBD results. This effect is also visible in the LS system: the shrinkage in Z direction for PEKK is larger than for PA12, whilst in X and Y direction such values are greater for PA12.

Having a lower shrinkage than Orgasol PA12, Kepstan 6000 PEKK is a promising candidate material for high temperature LS, showing 30% less shrinkage in LS than Orgasol PA12. These values can be further optimized by improving powder structure, such as shape and density. The results show the importance of powder properties not only for flowability and part density/consolidation but also for controlling shrinkage during cooling.

6. Data Availability

The datasets generated during the current study are not publicly available due to confidentiality reasons, but can be made available on reasonable request with the approval of all authors.

7. Acknowledgements

The authors would like to acknowledge the financial support of Arkema Innovations Chemistry for this study.

8. References

[1] ASTM International, ASTM F2792-12a: Standard Terminology for Additive Manufacturing Technologies, (2015).

[2] M. Attaran, The rise of 3-D printing: The advantages of additive manufacturing over traditional manufacturing, Business Horizons 60 (5) (2017) 677–688. doi:10.1016/j.bushor.2017.05.011.
URL http://dx.doi.org/10.1016/j.bushor.2017.05.011

[3] J. Y. Lee, J. An, C. K. Chua, Fundamentals and applications of 3D printing for novel materials, Applied Materials Today 7 (2017) 120–133. doi:10.1016/j.apmt.2017.02.004.

[4] D. Drummer, K. Wudy, F. Kühnlein, M. Drexler, Polymer Blends for Selective Laser Sintering: Material and Process Requirements, Physics Procedia 39 (2012) 509–517. doi:10.1016/j.phpro.2012.10.067.
URL http://www.sciencedirect.com/science/article/pii/S1875389212025941

[5] J. P. Kruth, G. Levy, F. Klocke, T. H. C. Childs, Consolidation phenomena in laser and powder-bed based layered manufacturing, CIRP Annals - Manufacturing Technology 56 (2) (2007) 730–759. doi:10.1016/j.cirp.2007.10.004.

[6] S. A. Tofail, E. P. Koumoulos, A. Bandyopadhyay, S. Bose, L. O'Donoghue, C. Charitidis, Additive manufacturing: scientific and technological challenges, market uptake and opportunities, Materials Today 21 (1) (2018) 22–37. doi:10.1016/j.mattod.2017.07.001.
URL https://doi.org/10.1016/j.mattod.2017.07.001

[7] M. Schmidt, M. Merklein, D. Bourell, D. Dimitrov, T. Hausotte, K. Wegener, L. Overmeyer, F. Vollertsen, G. N. Levy, CIRP Annals - Manufacturing Technology Laser based additive manufacturing in industry and academia, CIRP Annals - Manufacturing Technology (2017) 1–23doi:10.1016/j.cirp.2017.05.011.
URL http://dx.doi.org/10.1016/j.cirp.2017.05.011

[8] J. Sreedharan, A. K. Jeevanantham, Analysis of Shrinkages in ABS Injection Molding Parts for Automobile Applications, Materials Today: Proceedings 5 (5) (2018) 12744–12749. doi:10.1016/j.matpr.2018.02.258.
URL https://doi.org/10.1016/j.matpr.2018.02.258

[9] H. Hassan, N. Regnier, C. Pujos, E. Arquis, G. Defaye, Modeling the effect of cooling system on the shrinkage and temperature of the polymer by injection molding, Applied Thermal Engineering 30 (13) (2010) 1547–1557. doi:10.1016/j.applthermaleng.2010.02.025.
URL http://dx.doi.org/10.1016/j.applthermaleng.2010.02.025

[10] S. Negi, R. K. Sharma, Study on shrinkage behaviour of laser sintered PA 3200GF specimens using RSM and ANN, Rapid Prototyping Journal 22 (4) (2016) 645–659. doi:10.1108/RPJ-08-2014-0090.
URL http://www.emeraldinsight.com/doi/10.1108/RPJ-08-2014-0090

[11] N. Raghunath, P. M. Pandey, Improving accuracy through shrinkage modelling by using Taguchi method in selective laser sintering, International Journal of Machine Tools and Manufacture 47 (6) (2007) 985–995. doi:10.1016/j.ijmachtools.2006.07.001.

[12] S. P. Soe, D. R. Eyers, R. Setchi, Assessment of non-uniform shrinkage in the laser sintering of polymer materials, International Journal of Additive Manufacturing Technology 68 (2013) 111–125. doi:10.1007/s00170-012-4712-0.

[13] A. Mazzoli, Selective laser sintering in biomedical engineering, Medical and Biological Engineering 51 (2012) 245 – 256. doi:10.1557/mrs.2011.270.

[14] Y. Shi, Z. Li, H. Sun, S. Huang, F. Zeng, Effect of the properties of the polymer materials on the quality of selective laser sintering parts (2004).

[15] SpecialChem, Shrinkage (2019).
URL https://omnexus.specialchem.com/polymer-properties/properties/shrinkage

[16] ASTM, ASTM D955 - Standard Test Method of Measuring Shrinkage from Mold Dimensions of Thermoplastics (2014). doi:10.1520/D0955-08R14.

[17] EOS E-Manufacturing Solutions, Parameter sheet (2015).
URL http://www.sibtmk.ru/Pdf/EOS_PA2200_PrimeCast101.pdf

[18] Y. Shi, Z. Li, H. Sun, S. Huang, F. Zeng, Effect of the properties of the polymer materials on the quality of selective laser sintering parts, Journal of Materials: Design and Applications 218 (3) (2004) 247–252.
URL http://journals.sagepub.com/doi/pdf/10.1177/146442070421800308

[19] S. K. Tiwari, S. Pande, S. Agrawal, S. M. Bobade, Selection of selective laser sintering materials for different applications, Rapid Prototyping Journal 216 (21) (2015) 630–648. doi:10.1108/RPJ-03-2013-0027.

[20] A. Townsend, N. Senin, L. Blunt, R. K. Leach, J. S. Taylor, Surface texture metrology for metal additive manufacturing: a review, Precision Engineering 46 (2016) 34–47. doi:10.1016/j.precisioneng.2016.06.001.
URL http://dx.doi.org/10.1016/j.precisioneng.2016.06.001

[21] T. Grimm, G. Wiora, G. Witt, Characterization of typical surface effects in additive manufacturing with confocal microscopy, Surface Topography: Metrology and Properties 3 (1). doi:10.1088/2051-672X/3/1/014001.

[22] G. Strano, L. Hao, R. M. Everson, K. E. Evans, Surface roughness analysis, modelling and prediction in selective laser melting, Journal of Materials Processing Technology 213 (4) (2013) 589–597. doi:10.1016/j.jmatprotec.2012.11.011.
URL http://dx.doi.org/10.1016/j.jmatprotec.2012.11.011

[23] M. Van den Eynde, D. Strobbe, O. Verkinderen, L. Verbelen, B. Goderis, J.-P. Kruth, P. Van Puyvelde, Effect of thermal treatments on the laser sinterability of cryogenically milled polybutene-1, Materials Design 153 (2018) 15–23. doi:https://doi.org/10.1016/j.matdes.2018.04.072.
URL https://www.sciencedirect.com/science/article/pii/S0264127518303563

[24] L. Verbelen, S. Dadbakhsh, M. Van Den Eynde, J.-P. Kruth, B. Goderis, P. Van Puyvelde, Characterization of polyamide powders for determination of laser sintering processability, European Polymer Journal 75 (2016) 163–174. doi:10.1016/j.eurpolymj.2015.12.014.
URL http://dx.doi.org/10.1016/j.eurpolymj.2015.12.014

[25] R. D. Goodridge, C. J. Tuck, R. J. M. Hague, Laser sintering of polyamides and other polymers (2012). doi:10.1016/j.pmatsci.2011.04.001.

[26] D. Drummer, D. Rietzel, F. Kühnlein, Development of a characterization approach for the sintering behavior of new thermoplastics for selective laser sintering, Physics Procedia 5 (PART 2) (2010) 533–542. doi:10.1016/j.phpro.2010.08.081.

[27] J. Kruth, G. Levy, R. Schindel, T. Craeghs, E. Yasa, Consolidation of Polymer Powders by Selective Laser Sintering, in: International Conference on Polymers and Moulds Innovations, 2008, pp. 15–30.

[28] Y. Wang, J. D. Beard, K. E. Evans, O. Ghita, Unusual crystalline morphology of Poly Aryl Ether Ketones (PAEKs), RSC Adv. 6 (4) (2016) 3198–3209. doi:10.1039/C5RA17110E.
URL http://www.scopus.com/inward/record.url?eid=2-s2.0-84954170797&partnerID=tZOtx3y1

[29] A. J. Lovinger, D. D. Davis, Electron-microscopic investigation of the morphology of a melt-crystallized polyaryletherketone, Journal of Applied Physics 58 (8) (1985) 2843–2853. doi:10.1063/1.335856.

[30] K. H. Gardner, B. S. Hsiao, R. R. Matheson Jr., B. A. Wood, Structure, Crystallization and Morphology of Poly (aryl ether ketone ketone), Polymer 33 (12) (1992) 1752–1758.

[31] P. Avakian, K. H. Gardner, R. R. M. Jr., A comment on crystallization in PEKK and PEEK resins, Journal of Polymer Science Part C: Polymer Letters 28 (8) (1990) 243–246. doi:doi.org/10.1002/pol.1990.140280801.

[32] D. J. Blundell, A. B. Newton, Variations in the crystal lattice of PEEK and related para-substituted aromatic polymers: 2. Effect of sequence and proportion of ether and ketone links, Polymer 32 (2) (1991) 308–313. doi:10.1016/0032-3861(91)90019-F.

[33] M. Garcia-Leiner, D. P. Dennies, A. Yardimci, High Performance Polymers in Additive Manufacturing Processes: Un-

derstanding Process, Structure and Property, Microscopy and Microanalysis 21 (S3) (2015) 127–128. doi:10.1017/S1431927615001439.
URL http://www.journals.cambridge.org/abstract_S1431927615001439

[34] P. Chen, H. Wu, W. Zhu, L. Yang, Z. Li, C. Yan, S. Wen, Y. Shi, Investigation into the processability, recyclability and crystalline structure of selective laser sintered Polyamide 6 in comparison with Polyamide 12, Polymer Testing 69 (April) (2018) 366–374. doi:10.1016/j.polymertesting.2018.05.045.
URL http://linkinghub.elsevier.com/retrieve/pii/S014294181830624X

[35] B. Van Hooreweder, D. Moens, R. Boonen, J. P. Kruth, P. Sas, On the difference in material structure and fatigue properties of nylon specimens produced by injection molding and selective laser sintering, Polymer Testing 32 (5) (2013) 972–981. doi:10.1016/j.polymertesting.2013.04.014.
URL http://dx.doi.org/10.1016/j.polymertesting.2013.04.014

[36] Oxford University Press Inc., Polymer Data Handbook, New York, 1999.

[37] N. Hiramatsu, K. Haraguchi, S. Hirawaka, Study of Transformations among α, γ and γ' Forms in Nylon 12 by X-Ray and DSC, Japanese Journal of Applied Physics 22 (2R) (1983) 335.
URL citeulike-article-id:4540161%5Cnhttp://jjap.ipap.jp/cgi-bin/getarticle?magazine=JJAP&#38%5Cnvolume=22&#38%5Cnpage=335%5Cnhttp://stacks.iop.org/1347-4065/22/i=2R/a=335

[38] L. Li, M. H. Koch, W. H. De Jeu, Crystalline structure and morphology in nylon-12: A small- and wide-angle X-ray scattering study, Macromolecules 36 (5) (2003) 1626–1632. doi:10.1021/ma025732l.

[39] C. Ramesh, Crystalline transitions in Nylon 12, Macromolecules 32 (17) (1999) 5704–5706. doi:10.1021/ma990494o.

[40] L. Verbelen, S. Dadbakhsh, M. Van den Eynde, D. Strobbe, J.-P. Kruth, B. Goderis, P. Van Puyvelde, Analysis of the material properties involved in laser sintering of thermoplastic polyurethane, Additive Manufacturing 15 (2017) 12–19. doi:10.1016/j.addma.2017.03.001.

[41] A. Amado, M. Schmid, G. Levy, K. Wegener, Advances in SLS powder characterization, in: 22nd Annual International Solid Freeform Fabrication Symposium - An Additive Manufacturing Conference, Austin, 2011, pp. 438–452.

[42] S. Yang, J. R. G. Evans, Metering and dispensing of powder; the quest for new solid freeforming techniques, Powder Technology 178 (1) (2007) 56–72. doi:10.1016/j.powtec.2007.04.004.

[43] Arkema, Kepstan 6000 Series (2013).
URL https://www.arkema.com/export/shared/.content/media/downloads/products-documentations/incubator/arkema-kepstan-6000-tds.pdf

[44] T. Choupin, B. Fayolle, G. Régnier, C. Paris, J. Cinquin, B. Brulé, Isothermal crystallization kinetic modeling of poly(etherketoneketone) (PEKK) copolymer, Polymer 111 (2017) 73–82. doi:10.1016/j.polymer.2017.01.033.

[45] EOS, EOSINT P 800 (2003).
URL http://www.firechildren.org/pdfs/EOS_Plastiek.pdf

[46] EOS e-Manufacturing Solutions, Technical Description FORMIGA P 100 (2007).

[47] K. Senthilkumaran, P. M. Pandey, P. V. M. Rao, Shrinkage compensation along single direction dexel space for improving accuracy in Selective Laser Sintering, in: 4th IEEE Conference on Automation Science and Engineering, 2008, pp. 827–832. doi:10.1109/COASE.2008.4626479.

[48] H. J. Yang, P. J. Hwang, S. H. Lee, A study on shrinkage compensation of the SLS process by using the Taguchi method, International Journal of Machine Tools and Manufacture 42 (11) (2002) 1203–1212. doi:10.1016/S0890-6955(02)00070-6.

[49] O. R. Ghita, E. James, R. Trimble, K. E. Evans, Physico-chemical behaviour of Poly (Ether Ketone) (PEK) in High Temperature Laser Sintering (HT-LS), Journal of Materials Processing Technology 214 (4) (2014) 969–978. doi:10.1016/j.jmatprotec.2013.11.007.

[50] S. Ziegelmeier, F. Wollecke, C. Tuck, R. Goodridge, R. Hague, Characterizing the Bulk Flow Behaviour of LS Polymer

Powders (2013).

[51] L. Verbelen, J. Van Humbeeck, P. Van Puyvelde, Development of a method for pressure-free volumetric dilatometry of polymer melts and solids, Polymer Testing 69 (March) (2018) 219–224. doi:10.1016/j.polymertesting.2018.05.022.
URL https://doi.org/10.1016/j.polymertesting.2018.05.022

[52] M. Schmid, R. Kleijnen, M. Vetterli, K. Wegener, applied sciences Influence of the Origin of Polyamide 12 Powder on the Laser Sintering Process and Laser Sintered Parts, Applied Sc 7 (2017) 1–15. doi:10.3390/app7050462.

[53] S. Haeri, Y. Wang, O. Ghita, J. Sun, Discrete element simulation and experimental study of powder spreading process in additive manufacturing, Powder Technology 306 (2016) 45–54. doi:10.1016/j.powtec.2016.11.002.
URL http://dx.doi.org/10.1016/j.powtec.2016.11.002

[54] S. Ziegelmeier, P. Christou, F. Wöllecke, C. Tuck, R. Goodridge, R. Hague, E. Krampe, E. Wintermantel, An experimental study into the effects of bulk and flow behaviour of laser sintering polymer powders on resulting part properties, Journal of Materials Processing Technology 215 (1) (2015) 239–250. doi:10.1016/j.jmatprotec.2014.07.029.

[55] V. K. Vashishtha, R. Makade, N. Mehla, Advancement of Rapid Prototyping in Aerospace Industry -a Review 3 (3) (2011) 2486–2493.